

International Conference on Space Optics—ICSO 2014

La Caleta, Tenerife, Canary Islands

7–10 October 2014

Edited by Zoran Sodnik, Bruno Cugny, and Nikos Karafolas



Development of large aperture telescope technology (LATT): test results on a demonstrator bread-board

R. Briguglio

M. Xompero

A. Riccardi

F. Lisi

et al.



DEVELOPMENT OF LARGE APERTURE TELESCOPE TECHNOLOGY (LATT): TEST RESULTS ON A DEMONSTRATOR BREAD-BOARD

R. Briguglio¹, M. Xompero¹, A. Riccardi¹, F. Lisi¹, F. Duò⁵, C. Vettore⁵, D. Gallieni³, M. Tintori³, P. Lazzarini³,
C. Patauner⁴, R. Biasi⁴, F. D'Amato², M. Pucci², João Pereira do Carmo⁶

¹INAF, Oss. Astrofisico Arcetri, Italy

²INO, Istituto Nazionale di Ottica, Italy

³ADS, A.D.S. International, Italy

⁴MIG, Microgate, Italy

⁵OHB CGS, Compagnia Generale dello Spazio, Italy

⁶ESA, European Space Agency

ABSTRACT

The concept of a low areal density primary mirror, actively controlled by actuators, has been investigated through a demonstration prototype. A spherical mirror (400 mm diameter, 2.7 Kg mass) has been manufactured and tested in laboratory and on the optical bench, to verify performance, controllability and optical quality. In the present paper we will describe the prototype and the test results.

I. INTRODUCTION

The use of large primary mirrors as entrance aperture of optical systems for space applications is crucial to get higher image resolution in space missions of the next generation. As an example of innovative technologies in this field, active optics application appears very promising. The subject of the present paper is to report on the latest development of the project LATT (Large Aperture Telescopes Technology) which has the goal to explore the possibility to extend a well-established experience with ground-based optical telescopes to space-based missions. LATT is now at the end of phase 2 (ESA-ESTEC Contract No. 4200022321 CCN1), and it is the follow-up of the former project ALC (Advanced LIDAR Concept) started in 2007 in response to a different ESA contract, aimed to propose a space borne differential absorption Light Detection And Ranging system to measure water vapor distribution in atmosphere at 935.5 nm. In [1],[2],[3],[4],[7],[8] and [9] we described both the main concept and the past results we obtained with the former breadboard as we built and tested it for ALC and the preliminary design of the present breadboard we developed for LATT. This paper describes the main results we obtained measuring the breadboard performances.

The general concept we have been proposing since 2007 is based on 1-mm thickness glass mirror (Zerodur®), actively controlled to reach the specified shape after initial deployment, maintained within specs for the entire mission duration by means of a set of electromechanical actuators driven by a suitable electronic control that compute a correction matrix following the signal coming from an optical wave-front sensor. The closed control loop drives the mirror surface in the specified shape after the deployment, aligns the different segments in case of a segmented primary mirror and is able to keep the overall optical specification by mean of a suitable wave-front sensor with the help of a reference source over the full mission duration. The thin glass shell and the actuators are mounted on a very rigid and lightweight backplane, a CFRP-aluminum composite honeycomb structure. In order to maintain the structural integrity of the shell during the launch and the operations we are devising an electro-static "gluing" technique whose reliability is one of the main goals of the project.

Exploiting this conceptual elements, we designed a demonstrator - based on a thin glass (Zerodur®) mirror, 400mm diameter - to study the concept of a primary mirror with a mass areal density less than 18 kg/m², a residual optical error less than 156 nm, and a local power dissipation of the order of a few watts.

II. OBB DESCRIPTION AND MANUFACTURING:

The Optical demonstrator Bread Board (OBB) is composed by a backplane, 19 actuators, the controlling electronics and a 400mm glass thin shell (TS). The total system mass is 2686 g, giving an areal density of 18 kg/m². A summary of such main components is presented hereafter.

A. OBB Backplane:

The OBB backplane (or Reference Body, RB) is a sphere sector with a 5000 mm curvature radius to match the glass shell shape. The RB size is 440 mm diameter and is made up of a honeycomb sandwich with Carbon Fiber Reinforced Plastic (CFRP) sheets and an aluminum core. The CFRP has been selected as candidate material for the RB because of its low density, high stiffness, low Coefficient of Thermal Expansion (CTE) and vacuum compatibility. The actuator electronic boards (or cups) are inserted in 19 passing-thru holes, 60 mm diameter, drilled in the sandwich according to a circular geometry with 2 rings and a central actuator. The sandwich mass

is 2000 g, plus three aluminum mounting plates of total mass 1040 g. The front surface is aluminized to provide a conductive plate for the electrostatic locking (EL) and protected with SiO₂.

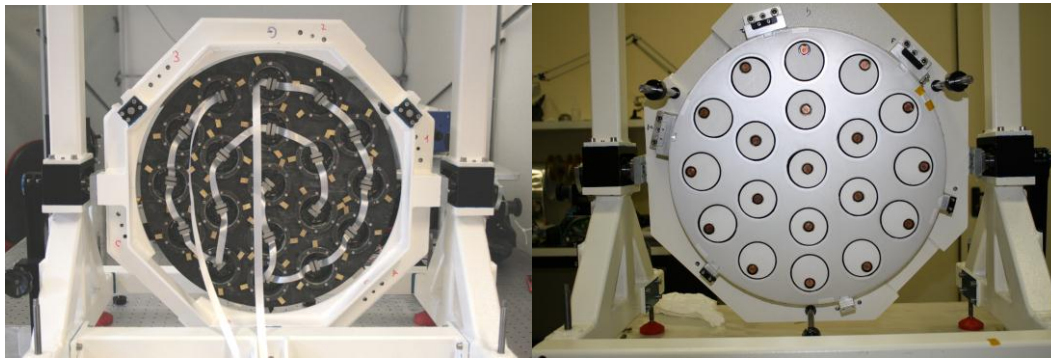


Fig 1 OBB Backplane final assembly. Left: back view. Right: front view on the optical bench test stand.

B. Control electronics

The OBB control electronics comprehends a central control unit and the actuator control electronics, co-located with each actuator in the actuator cups. The central control unit is based on the Microgate *Basic Computational Unit* (BCU) board and the *Signal Generator* (SigGen) board that have been already successfully implemented in the LBT and VLT projects [10]. The OBB is commanded from a workstation via Ethernet to a Basic Computational Unit board (BCU) and from there via two LVDS buses to the smart actuator boards (SAB) in each actuator cup.

The timing of the ADC sampling and the tasks that have to be performed in each microcontroller (MCU) on the SAB is controlled by a DSP on the BCU.

The MCU on each SAB performs the following tasks:

- Communication between BCU and SAB (with CRC check) and processing of the received commands
- Reading the ADC samples from the capacitive sensor signal conditioning circuitry
- Linearization of the ADC values
- Calculation of the coil current using an integer based PID control
- Setting the DAC that controls the coil driver.

The local control loop on each of the 19 actuators that holds the mirror in the desired position works with a frequency of 1.8kHz.

C. OBB actuators:

The actuators control electronics SAB is specifically designed to be as much as possible representative of a future 'flying unit', both in terms of interfaces, size, weight, power dissipation and control performances. The SABs contain the front-end electronics for each actuator and are connected to the coil and the capacitive sensor armature on one side and to the BCU on the other side. These boards perform the local loop that controls accurately the gap between the RB and the shell by means of contactless, voice coil force actuators and capacitive sensors.

The SAB comprehends four main subsystems: capacitive sensor, voice coil motor current driver, microcontroller based control unit and auxiliary electronics, including the power supply regulators and voltage references and the communication interface. From the hardware point of view all the 19 SABs are identical. The SAB is placed in the actuator receptacle (actuator "cups") on three elevations inside the actuator cups fixed with three screws. The electrical devices are mounted all on the surface of the PCB and three wires are guided through two holes down to the coil and CapSens armature of the cup. The SAB cable connectors are held by two latch/ejector connectors mounted on each SAB and fixed on the bottom face of the OBB structure between the cups to minimize the free length when the system is subjected to vibration. At the end a visual inspection of each SAB under the microscope was performed in order to verify the quality of the solder spots and the cleanness of the boards. The 19 actuators were connected to the two buses A and B using vacuum suitable flat cables. 9 SABs were connected to one bus and 10 SABs to the other bus. Each SAB is supplied with 3.3V and 5V through the bus lines.

D. OBB Shell:

The OBB shell has been manufactured starting from Zerodur disks (selected quality, class 4), with 42 cm diameter and 1.5 cm thickness. The first side to be produced has been the concave one. After polishing the

concave surface, the thick shell has been glued to a convex Zerodur mould, 5 m curvature radius, by using a thermal glue. Then the shell diameter has been reduced to 40 cm, and the thickness to about 1.6 mm.

Finally, the polishing procedure of the convex side has led to the final thickness of 1 mm with the right surface quality. The shell has been detached from the mould, and then cleaned for coating. After detachment the shell has been held by rubber moulds, with the proper shape.

The shell thickness has been verified, both during and after polishing, by using an optical gauge (Precitec CHRcodile S), and the final surfaces quality by using a Zygo NewView 5000 3D surface profiler. The shell has been subsequently coated with Unprotected Aluminum. The following picture shows the coated shell equipped with the 6 membranes and the magnets.

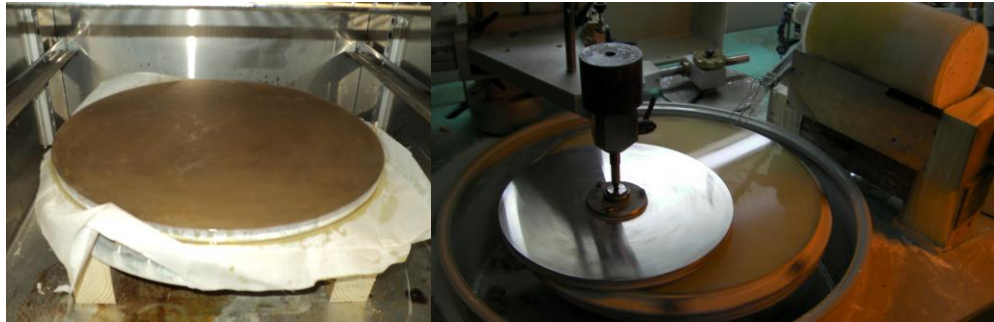


Fig 2 Left: The thick shell, just glued onto the zerodur mould (under the tissue). Right: Polishing of the concave surface

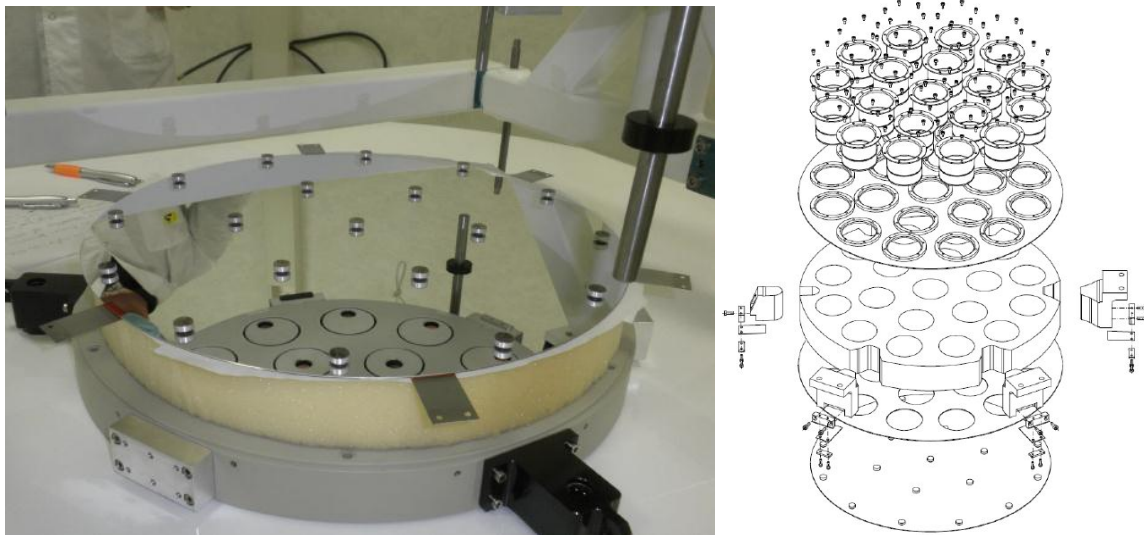


Fig 3 Left: Coated shell with magnets and membranes. Right: exploded view of the OBB.

III. QUALIFICATION TEST CAMPAIGN

A. ELECTRO MECHANICAL PERFORMANCE TEST

An electromechanical verification of the OBB actuators has been carried out in Microgate to verify the controllability of the active mirror. After the assembly of the OBB the control performance of the system was tested in terms of **position reading noise** and **modal step response**. The performance of the CapSens reading is checked by acquiring 512 linearized distance values.

The resulting PSD and integral PSD of the CapSens test with the shell positioned at a distance to the reference body of 700 μ m is shown in Fig 4.

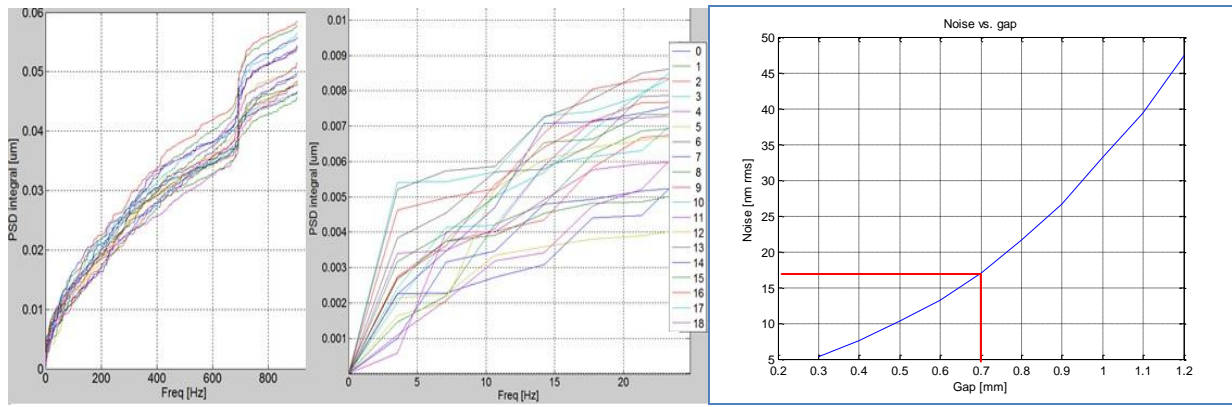


Fig 4 Left: Integral PSD of CapSens reading and zoom. Right: CapSens noise vs. gap between shell and actuator.

The position update command for the shell will arrive with a frequency of less than 1Hz (large motion bandwidth). Applying a margin factor of 10, concerning the position stability we are actually interested in the noise spectral content up to 10 Hz. A zoom of the PSD integral in this frequency range (see Fig 4 Left) shows that the capacitive sensor noise is within the value predicted by design: as shown in Fig 4 left a noise of <6 nm RMS has been measured at 10Hz while the expected value was 16 nm as can be seen in Fig 4 right.

Further the dynamic performance of the mirror control has been tested. First the interaction matrix between capacitive sensor reading and forces applied by the voice coils has been acquired by applying piston commands to each actuator. This interaction matrix corresponds approximately to the stiffness matrix of the mirror sampled at the actuators positions. By factorizing this matrix through Singular Value Decomposition we computed the electromechanical modes of the mirror. Then the modal step response time was measured by commanding each of the 19 resulting electromechanical modes.

According to the specification, the settling time within 99% of the commanded value should be less than 0.72s corresponding to 1Hz large motion bandwidth. The results presented hereafter are again acquired with the mirror in relaxed position at 700µm gap from the reference body. As can be seen in Fig 5, the specification can be achieved for the first 15 modes. Concerning the higher modes, the shell stiffness is too high when compared with the control proportional term, so the dynamic response is dominated by the integral term and therefore slower. The settling time does not change significantly even when the shell is previously tilted horizontally or vertically by the actuators before applying the modes. This results show a good controllability of the deformable mirror with a performance very close to the expectations and specifications.

The power consumption of the actuator electronics with an RMS coil force of a few tens of mN to hold the shell in its natural position is 79mW per SAB, which is just slightly higher than the value of 72mW expected by design.

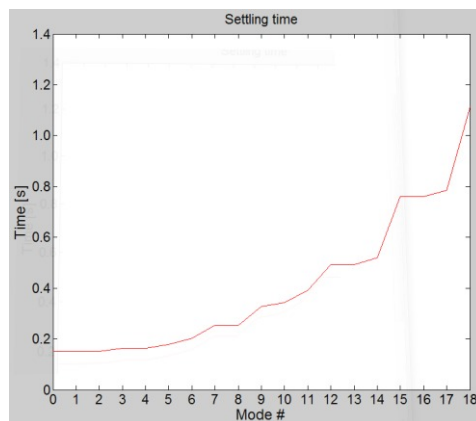


Fig 5 Settling time of the electromechanical modes

B. OPTICAL CALIBRATION IN 1g ENVIRONMENT:

The OBB was subjected to a 1 month optical test campaign at the INAF-Osservatorio Astrofisico Arcetri, in the adaptive optics (AO) laboratories. The test was devoted to the system optical qualification in a 1g, laboratory conditions environment, before the thermo-vacuum tests. Here, we will briefly recall some general

points about the optical calibration of a deformable mirror (DM) for AO: some references (related to the Large Binocular Telescope and Very Large Telescope DMs) may be found in [5] and [6].

As explained in the previous sections, the OBB is controlled by mean of a Feed Forward or stiffness matrix, whose eigenfunctions are the system stiffness modes; such functions provide a natural control basis for the system. The key-point of the calibration is the collection of the optical shape of each of the mirror eigenvectors. Such shapes are commonly known as *influence functions* (IF) and are grouped together in the *optical interaction matrix* (IM), which provides a suitable transformation operator connecting the actuators space to the wavefront (WF) one; the system is linear, so that any WF pattern (as seen by an interferometer, e.g.) may be decomposed within the actuator fitting error into a linear combination of mirror modes and nulled with the opposite actuator command. The IF may be sampled by measuring stiffness modes or single actuator commands, equivalently.

Optical test set-up

The OBB has been installed on the optical test bench, providing mechanical insulation from the ground, and covered with foam sheets to minimize convection effects. The OBB is installed vertically on the bench and it is tested at its center of curvature. The illumination optics is composed by a F/12 beam expander and 3 flat mirrors to fold horizontally the 5m measuring arm. The interferometer is a Twyman-Green, 4D Technology, dynamic device; it is able to measure phasemaps in a single frame with a typical exposure time of tens of microseconds, allowing the rejection of vibration noise. The very large capture range (250 fringes on the CCD frame) resulted very useful to measure the warped mirror edges at the very beginning of the test.

The thin shell (TS) is hold vertically by mean of 6 flexures, which are glued on the front side of the glass and connected to the reference body (RB); they are requested for operation in 1g environment to provide a vertical support and also a lateral constraint to the mirror while in close loop. Such condition is however different with respect to the nominal one, where only the lateral constraint is required. The combined effect of gravity and over-constraint to the TS is to add a static deformation pattern, which was observed to be well beyond the interferometer capture range (tens of micron, over an area of the actuator pitch) at the very beginning of the optical test. To partially compensate for such bending, 3 flexures out of 6 were removed and the remaining 3 ones were fine-positioned by shimming their mounting points.

Flattening process

The initial TS shape was controlled by applying the first 5 mirror stiffness modes with arbitrary amplitude, in a trial-and-error process to maximize the visible area. Once most of the TS was visible, the mirror IF were measured. The sampling procedure is based on a differential technique: each mode is applied and measured in a sequence of positive and negative commands, iterated at the maximum frame rate allowed by the mirror settling time. Such procedure is valuable to reduce the convection noise and to suppress static patterns. The same procedure was adopted to measure the individual actuator IF. The command amplitude for each mode is selected in order to maximize the SNR and to avoid saturating the actuator forces: typical values are within the range 200 nm RMS to 600 nm RMS, to be compared with a typical measurement noise of 10 nm RMS. The resulting images are presented in Fig 6.

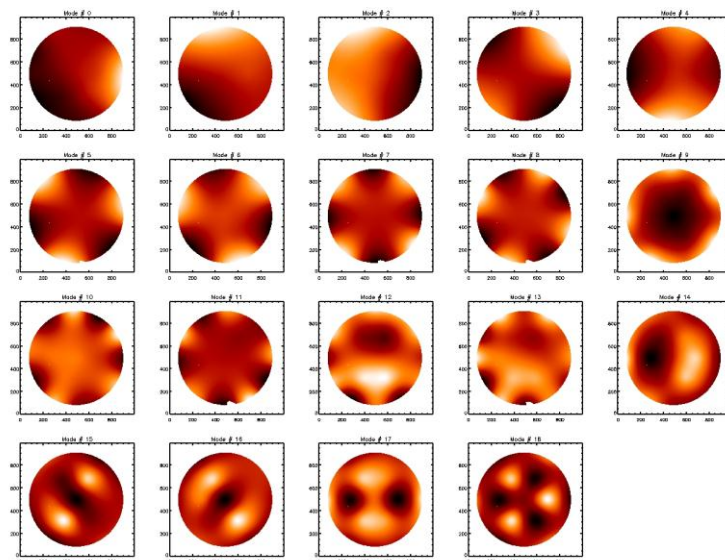


Fig 6 Optical shape of the 19 mirror stiffness modes, ordered by increasing stiffness value.

The flattening is based on the current WF decomposition into modes of the IM; the WF is then corrected by applying the corresponding combination of mirror modes with negative amplitude. The procedure is affected by accuracy error, given mostly by air convection: such contribution is minimized by time integration of the phasemap. The flattening result is shown in Fig 7: in the left panel the final WF is presented and in the right one the corresponding actuator forces are shown. The residual figuring is mostly given by the flexure induced deformations, which are poorly matching the actuators geometry and cannot be compensated with the flattening. The flexures location is easy recognizable from the rectangular masks in the image. The peak force is lower than 1/3 of the force budget.

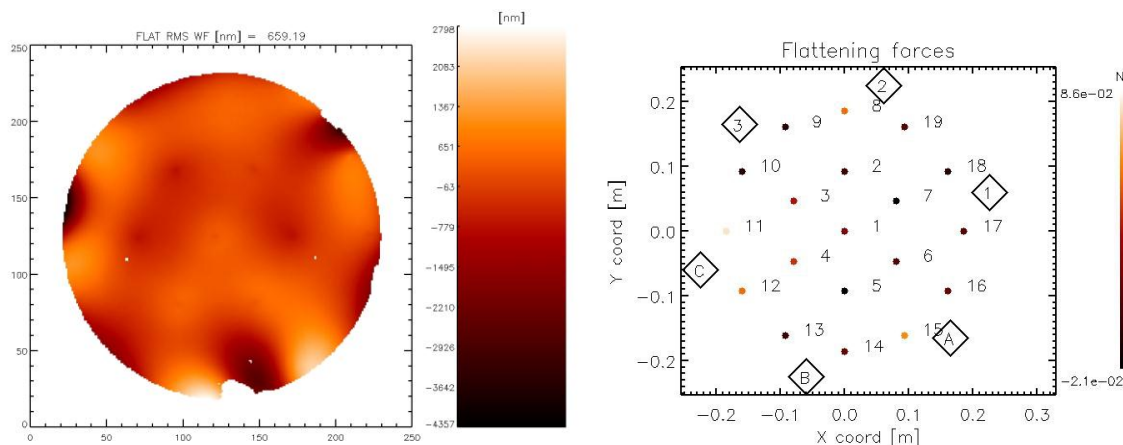


Fig 7 Left: flattening result, measured on the full 400 mm diameter pupil. Right: actuator forces requested for the flattening. The boxes indicate the flexure locations.

As most of the residual deformation is located at the TS edges, we tested the flattening command on a reduced optical area: this consists in masking out an arbitrary outer ring and rejecting that information from the computation of the flattening command. The selected diameter values and resulting WFE are listed in Table 1. For the considered realizations, we least-square fitted the theoretical flexure deformations from finite element model (FEM), provided by ADS. These data consists in the shell deformation expected from each flexure when perturbing tits 6 degrees of freedom, after excluding the least significant ones. The FE data have been properly aligned to match the mirror geometry in the images, then they have been fitted and subtracted from each flattening realization. The results are listed in

Table 1 at column three. The values show clearly that the subtraction procedure works fine on the inner portion of the mirror, while it fails all along the external ring. In our opinion this fact originates from the design of the flexure's constraint which applies such so strong forces and torques to the thin shell, to make a linear representation of the mechanical interactions only a first-grade approximation to the physics of the mirror.

Diameter (mm)	WFE flat (nm RMS)	WFE FEA-subtr. (nm RMS)
400	659	301
368	616	218
325	327	130
296	197	87
265	114	57
234	66	43
182	35	27

Table 1 Flattening results on a smaller optical area. Right column: residual after the subtraction of the flexures FE data.

C. ELECTRO STATIC LOCKING TEST:

The Electrostatic locking works between the back surface of the thin shell and the front surface of the carbon-fiber backplate structure. The shell surface is coated by unprotected aluminium layer with typical thickness 0.1

micron to make one of the armatures of the capacitor. This surface is put in electrical contact with the mirror optical one and the whole assembly is grounded.

The backplane front face is also coated by a layer of protected aluminum, that is 0.1 micron of aluminum plus 4 micron of SiO₂, which makes the insulating dielectric layer.

In order to provide the necessary pressure restraint between these two parts at acceptable differential voltage, the two surfaces shall match within few microns. This is especially true at the low and medium spatial scales, while the mirror shell is sufficiently compliant (flexible) to conform to the backplane on the low order shape errors. Once the voltage was applied to both armatures, we tested the functionality of the Electrostatic locking by applying a lateral force to the shell edge and by measuring it through a load cell. As soon as the measured forces drops and the shell slides away we have a quantification of the electrostatic (shear) pressure as a function of the applied voltage.

The friction coefficient between the two armatures is conservatively assumed equal to 1. Therefore, the same measured pressure can be compared to the design level computed to withstand the inertial forces perpendicular to the mirror that occur at launch.

The demanded pressure to withstand 57g static equivalent accelerations normal to the optical surface is 2300 Pa. In order to avoid putting at risk the shell integrity, the lateral force applied was bound under 40 N: the test was then aimed to estimate the gain between the achieved Lateral Restraint Force and the applied Voltage and to use this to infer the demanded operational voltage.

During the test we have monitored the current flowing between the two armatures to determine the max applied voltage before breaking the dielectric: up to 120 V the current remained below 0.05 mA, which was considered a measurement bias. At 150 V after some minutes this current started to increase up to 0.8 mA showing that the insulation was starting to leak somewhere.

The Electrostatic locking functional test gave finally the following results:

1. 120 V seems a level sustainable by the system, above that some current leakage between the armatures occurred;
2. significant improvement of the retention force to voltage gain was achieved once a high voltage level (150V and 100 V) was applied for 5 min before the test was carried out;
3. the gain measured in this way led to an operational voltage comparable to the design value below 150 V.
4. a minimum voltage around 60 V is anyway needed to keep alive the Electrostatic locking effect, under such voltage lateral restraint force measure was not repeatable;
5. no adhesion effect due to trapped air was observed, that is once the voltage was drop the retention force vanished; therefore these results should be repeatable in vacuum too.

Based on such findings it seems reasonable to set the Electrostatic locking operational voltage to 120 V.



Fig 8 The operator (ADS) applies a lateral force to the shell edge that is measured through a load cell.

IV. CONCLUSIONS

The trend toward higher image resolution in space applications calls for the study of new technologies aimed to obtain the requested optical performance beyond the classical optical systems, in a tight frame of mass (and cost) budget. Aiming to this purpose, we have been proposing since 2007 a new concept of lightweight optics, based on a rigid backplane where a set of electromechanical actuators, under the control of hardware running suitable algorithms which elaborate the signal coming from the wave front sensor, drive a thin glass mirror. The prototype we designed and built under the LATT contract shows the solidity of the concept.

The LATT OBB is a 400 mm diameter prototype mirror, manufactured to demonstrate the concept of low-dissipation, lightweight active mirror for large aperture space telescopes. The prototype includes a glass shell

1mm thick and a CFRP and aluminum honeycomb reference body and is controlled by 19 contactless, voice coil actuators. The areal mass density is a paramount importance parameter to keep under control the budget of any spatial mission. In our case, without any special optimization effort and due to the intrinsic properties of the concept, we got a value of about 18 kg/m^2 , we compare very well with existing projects.

The mirror was subjected to electromechanical and optical tests, extensively described in the present paper. The measurement tests we performed on the OBB demonstrated that the optical quality of the spherical mirror over a surface 325mm diameter is well inside the required figure. This result is even more remarkable when we observe we did not undertake any specific design effort to conceive the mechanical constraints that keep the mirror during the optical test, so that the outer ring of the mirror surface is heavily deformed in the 1-g environment. The control loop, that is the driving electronics, the computing hardware, and the controlling algorithms is very stable, we do not see any stumbling block in the process to modify the electronics design for space applications. In particular, the internal metrology noise is 6 nm RMS and the modal settling time is lower than 1.1s for all the stiffness modes (lower than 0.75s for the first 15 modes). The overall bandwidth of the control loop is compatible with the 10-Hz requirement; there is the possibility to tune the control parameters to get better performance. The power dissipation on the actuator set is limited, due to the low force budget that the actuators are called to give in condition of static correction; the dissipated power per actuator is 79 mW.

An electrostatic locking procedure, to preserve the integrity of the thin shell from the launch vibrations. has been identified and successfully tested in ambient. The qualification test campaign will be continued with the environmental test phase namely thermal vacuum and vibration testing.

The OBB Environmental thermal tests, by no means intended to be representative of any space qualification process, shall be very useful to prove the functionality of the proposed design under flight thermal environmental conditions. In addition Electrostatic Locking (EL) shall be proven under vacuum conditions as well.

Finally the vibration test shall definitely confirm the mirror survivability to launch via Electrostatic Locking (EL), this latter being identified in the study phase as one of the most critical area to be verified

REFERENCES

- [1] F. Simonetti, A. Zuccaro Marchi, L. Gambicorti, P. Mazzinghi, V. Bratina, Large aperture telescope for advanced lidar system, *Optical Engineering*, 49 (2010) 7-30
- [2] Mazzinghi P., Bratina V., Ferruzzi D., Gambicorti L., Simonetti F., Zuccaro Marchi A., Salinari P., Lisi F., Olivier M., Bursi A., Gallieni D., Biasi R., Pereira J. "Deployable, lightweight and large aperture spaceborne telescope for LIDAR based earth observations" PROC. SPIE, Lidar Technologies, Techniques, and Measurements for Atmospheric Remote Sensing III, Upendra N. Singh; Gelsomina Pappalardo, Ed. Oct 2007, Vol. 6750, p. 67500X-1- 67500X-9.
- [3] Mazzinghi P., Bratina V., Ferruzzi D., Gambicorti L., Simonetti F., Zuccaro Marchi A., Salinari P., Lisi F., Olivier M., Bursi A., Gallieni D., Biasi R., Pereira J. "Lightweight active controlled primary mirror technology demonstrator" PROC. SPIE, Lidar Technologies, Techniques, and Measurements for Atmospheric Remote Sensing III, Upendra N. Singh; Gelsomina Pappalardo, Ed. Oct 2007, Vol. 6750, p. 67500Y-1- 67500Y-10.
- [4] P. Mazzinghi, V. Bratina, D. Ferruzzi, L. Gambicorti, F. Simonetti, A. Zuccaro Marchi, P. Salinari, F. Lisi, M. Olivier, A. Bursi, J. Pereira, "An ultra-lightweight, large aperture, deployable telescope for advanced lidar applications", *Proceeding ICSO 2006 Sixth International Conference on Space.*, ESA/ESTEC Noordwijk, Netherlands 27-30/06/ 2006
- [5] Riccardi, A., Xompero, M., Briguglio, R. & al, "The adaptive secondary mirror for the Large Binocular Telescope: optical acceptance test and preliminary on-sky commissioning results", *Proceedings of the SPIE*, Volume 7736, pp. 77362C-77362C-12 (2010)
- [6] R. Briguglio, R. Biasi, M. Xompero, A. Riccardi, et al.: "The deformable secondary mirror of VLT: final electro-mechanical and optical acceptance test results", *Proceedings of the SPIE*, AS14, 9148-153, Press.
- [7] A. Zuccaro Marchi *et al.* "A technology demonstrator for development of ultra-lightweight, large aperture, deployable telescope for space applications", *Proc. of the 7th ICSO*, Toulouse, France, October 2008.
- [8] A. Zuccaro Marchi *et al.* "Technological Developments for Ultra Lightweight , Large Aperture, deployable mirror for space telescopes", *Proc. of the 8th ICSO*, Rhodes, Greece, October 2010.
- [9] Gambicorti L., D'Amato F., *et al.* "Last Results of technological developments for ultra-lightweight, large aperture, deployable mirror for space telescopes", *Proc. of the 9th ICSO*, Ajaccio, France, October 2012.
- [10] Biasi, R.; Andrighettoni, M.; Riccardi, A.; Biliotti, V.; Fini, Luca; Mantegazza, P.; Gallieni, D., "Dedicated flexible electronics for adaptive secondary control", *Advancements in Adaptive Optics*. Edited by Domenico B. Calia, Brent L. Ellerbroek, and Roberto Ragazzoni. *Proceedings of the SPIE*, Volume 5490, pp. 1502-1513 (2004)